

PAPER

[View Article Online](#)
[View Journal](#) | [View Issue](#)

Bio-sorbable, liquid electrolyte gated thin-film transistor based on a solution-processed zinc oxide layer

Mandeep Singh,^a Gerardo Palazzo,^b Giuseppe Romanazzi,^c
Gian Paolo Suranna,^d Nicoletta Ditaranto,^e Cinzia Di Franco,^f
Maria Vittoria Santacroce,^g Mohammad Yusuf Mulla,^h Maria Magliulo,ⁱ
Kyriaki Manoli^j and Luisa Torsi^{*k}

Received 25th April 2014, Accepted 9th May 2014

DOI: 10.1039/c4fd00081a

Among the metal oxide semiconductors, ZnO has been widely investigated as a channel material in thin-film transistors (TFTs) due to its excellent electrical properties, optical transparency and simple fabrication via solution-processed techniques. Herein, we report a solution-processable ZnO-based thin-film transistor gated through a liquid electrolyte with an ionic strength comparable to that of a physiological fluid. The surface morphology and chemical composition of the ZnO films upon exposure to water and phosphate-buffered saline (PBS) are discussed in terms of the operation stability and electrical performance of the ZnO TFT devices. The improved device characteristics upon exposure to PBS are associated with the enhancement of the oxygen vacancies in the ZnO lattice due to Na⁺ doping. Moreover, the dissolution kinetics of the ZnO thin film in a liquid electrolyte opens the possible applicability of these devices as an active element in "transient" implantable systems.

^aDipartimento di Chimica Università degli Studi di Bari Aldo Moro, Via Orabona 4, 70126 Bari, Italy

^bDipartimento di Chimica Università degli Studi di Bari Aldo Moro, Via Orabona 4, 70126 Bari, Italy

^cDICATECH: Dipartimento di Ingegneria Civile, Ambientale, del Territorio, Edile e di Chimica, Polytechnic of Bari, Campus Universitario, via Orabona 4, 70125 Bari, Italy

^dDICATECH: Dipartimento di Ingegneria Civile, Ambientale, del Territorio, Edile e di Chimica, Polytechnic of Bari, Campus Universitario, via Orabona 4, 70125 Bari, Italy

^eDipartimento di Chimica Università degli Studi di Bari Aldo Moro, Via Orabona 4, 70126 Bari, Italy

^fCNR-IFN and Dipartimento Interateneo di Fisica, Università degli Studi di Bari "A. Moro", Via Orabona, 4, 70126, Italy

^gCNR-IFN and Dipartimento Interateneo di Fisica, Università degli Studi di Bari "A. Moro", Via Orabona, 4, 70126, Italy

^hDipartimento di Chimica Università degli Studi di Bari Aldo Moro, Via Orabona 4, 70126 Bari, Italy

ⁱDipartimento di Chimica Università degli Studi di Bari Aldo Moro, Via Orabona 4, 70126 Bari, Italy

^jDipartimento di Chimica Università degli Studi di Bari Aldo Moro, Via Orabona 4, 70126 Bari, Italy

^kDipartimento di Chimica Università degli Studi di Bari Aldo Moro, Via Orabona 4, 70126 Bari, Italy. E-mail: luisa.torsi@uniba.it; Fax: +39 0805442092; Tel: +39 0805442092

1. Introduction

Over the years, semiconductor oxide-based thin-film transistors have attracted a great deal of attention due to their high charge-carrier mobility, transparency and excellent chemical and mechanical stability.^{1–3} Indeed, transparent electronics have gained attention during the last few years and are today established as one of the most promising technologies for the next generation of flat panel displays due to the excellent electronic performance of many wide band-gap semiconductor oxides. In particular, zinc oxide (ZnO) is an interesting and promising material as it holds a favorable combination of properties, including excellent transparency in the visible range, good electronic properties, even when processed from solution, and strong piezoelectric properties.^{4,5} Last but not least, ZnO is biocompatible^{6,7} and biodegradable, while zinc is among the most abundant elements in the earth's crust. All these make ZnO a key functional material with versatile properties for important applications in sensing, catalysis, optical emission, piezoelectric transduction and actuation.⁸ It would be also suitable as an active layer in electronic devices that can be integrated in a living organism, even in the human body.

High-performance metal oxide TFTs are typically manufactured by vacuum-processing methods, such as radio frequency magnetron sputtering and pulsed laser deposition, which pose some limitations in mass production for the realization of low-cost optoelectronic applications. Solution-processable oxide semiconductors indeed represent a fast-emerging technology that holds promise in the area of TFT applications. Recently, significant research effort has been devoted to developing novel materials and methodologies to improve electronic transport figures of merit, as well as to actuate processing at low temperature to ensure compatibility with plastic or even biodegradable paper or silk substrates.^{3,9,10} For this reason, a large research effort has been dedicated to the development of solution-processing methods for the fabrication of oxide TFTs, including ZnO TFTs.^{11–14} Studies in this direction involve ultraviolet photochemical activation of sol-gel precursors,^{15,16} sol-gel on chip,¹⁷ along with a number of colloidal nanoparticle-based approaches.^{18,19} The use of preformed colloidal metal oxide nanocrystals and nanoparticles (NPs) offers advantages, but the high melting temperatures, along with the presence of highly insulating carbon-based surfactants, lead to transistors with modest performance levels even at relatively high sintering temperatures.¹⁸ Recent advances in sol-gel-based methods have, on the other hand, enabled the development of oxide-based TFTs with electron mobilities as high as $11 \text{ cm}^2 \text{ V}^{-1} \text{ s}^{-1}$ at 250°C .¹⁷ A very interesting approach has been also proposed that sees high-performance ZnO transistors processed *via* an aqueous carbon-free metal oxide precursor route at temperatures between 80 and 180°C .²⁰

Lately, the concept of gating TFTs with an ionic conducting electrolyte,^{21,22} rather than with an insulating dielectric, has been put forward as it allows for low voltage operation directly through a droplet of pure water,²¹ but also by means of a high ionic strength fluid in contact with a TFT channel, this making such devices very promising also for bio-organic electronic applications.²³ In electrolyte-gated TFTs (EG-TFTs), the electrolyte serves as a dielectric being positioned, as customary, between the gate electrode and the semiconductor active channel

material. In a typical n-type EG-TFT device, when a positive gate bias is applied, the anions migrate towards the gate–electrolyte interface and the cations migrate towards the semiconductor–electrolyte interface, leaving a charge-neutral electrolyte in between them. This ion migration leads to a net charge accumulation at the gate–electrolyte (negative charges) and semiconductor–electrolyte (positive charges) interfaces, generating, at the steady state, two electrical double layers (EDLs), one at each interface, with all the applied voltage that drops across the EDLs. The total capacitance of the electrolyte gating layer, determined by the capacitance of the two EDLs connected in series, is dominated by the smaller of the two single EDLs. The value of capacitance is typically on the order of $10\text{ }\mu\text{F cm}^{-2}$, thus making it possible to induce a very large charge carrier concentration ($\sim 10^{15}\text{ cm}^{-2}$) in the transistor channel at relatively low applied gate voltages ($<3\text{ V}$).²¹ In addition, as the static capacitance of the electrolyte is virtually independent from the thickness of the electrolyte layer, even a thick layer will attain low-voltage operation, but also the device figures of merit are independent from thickness inhomogeneities.

This approach has also been used to gate ZnO-based TFTs, mostly through solid ionic polymers and gels, as well as ionic liquids. Interestingly, solid electrolyte-gated ZnO TFTs have been used to fabricate an inverter circuit by printing on a plastic substrate.²⁴ In this case, high-mobility, low-voltage ZnO TFTs on a kapton substrate were fabricated by aerosol jet printing, this being a versatile method for patterning a wide range of electronically functional liquid inks.²⁵ To achieve low-voltage operation a printable high-capacitance ($3.80\text{ }\mu\text{F cm}^{-2}$) ion-gel solid electrolyte was used, as previously proposed.²⁶ Such gating materials allow operation of the device below 2 V in a nitrogen environment, reaching a field effect mobility and threshold voltage of $1.67\text{ cm}^2\text{ V}^{-1}\text{ s}^{-1}$ and 0.97 V , respectively. A similar contribution has been published regarding an amorphous ZnO channel gated through an ionic liquid tape.²⁷ Other contributions concerning ZnO-based TFTs gated through solid electrolytes such as ionic liquids^{28,29} or composite solid polymers can be found. In the latter case a ZnO single nanowire is used as the active element of the channel, and the field-effect mobility and the threshold voltage of a typical ZnO single-nanowire transistor are $62\text{ cm}^2\text{ V}^{-1}\text{ s}^{-1}$ and 0.93 V , respectively.³⁰ Interestingly, the electrochemical gating approach is shown not to limit the switching speed of the device, as a frequency in the range of 100 kHz is already achievable with an in-plane transistor geometry. Moreover, unlike the ionic liquids, the composite solid polymer electrolyte studied in this work is found to be stable under ambient conditions and the transistors have shown no noticeable degradation after an exposure of 3–4 weeks in air. More recently, an innovative contribution proposed by Grell's group reported a ZnO electron transporting thin-film transistor directly gated through a drop of pure water.³¹ To minimize the impact of water on the stability of the thermally converted precursor route ZnO, the surface was modified by an hexamethyldisilazene hydrophobic layer. Assuming a capacitance per unit area (C_i) of $3\text{ }\mu\text{F cm}^{-2}$ measured on a water-gated polythiophene TFT,²¹ an electron mobility as high as $8.8\text{ cm}^2\text{ V}^{-1}\text{ s}^{-1}$ was found, similar to the $5.25\text{ cm}^2\text{ V}^{-1}\text{ s}^{-1}$ reported for a “dry-gated” precursor-route ZnO TFT.³² On the other hand, much inferior figures of merit are found by using a small gate area. This can be rationalized considering that a gate capacitance, comparatively higher than the ratio between the channel and gate contact area, should be in place to assure the same level of performance.³³

As already outlined, one of the relevant aspects of ZnO structures is their biocompatibility. ZnO nanoparticles are indeed believed to be nontoxic, bio-safe and biocompatible, as proven by their use for many every-day life applications, such as drug carriers and cosmetics. For instance, a study on the biocompatibility of ZnO nanowires at the cellular level has shown that they are completely biocompatible, bio-safe and are ranked as reliable and trustworthy for applications in biomedicine and engineering.⁸ Moreover, the biodegradability and biocompatibility of ZnO nanowires or nano-belts, which is crucial for the application of ZnO nanostructures in biosensing, has been also assessed.³⁴ A novel and extremely interesting approach foresees the use of water-sorbable devices and circuits^{35–37} to be used as implantable “transient” opto-electronic systems. Not only has ZnO been shown to dissolve in water and in an electrolyte,³⁴ but ZnO devices have even been fabricated on silk or paper substrates that quickly vanish by simple dissolution. Each constituent material disappears due to hydrolysis at different rates, and the time frames for dissolution can be programmed not only by encapsulation and packaging methods, but also by choices of dimensions, thicknesses and configurations in the materials for the device structures. These “transient” devices and circuits could be used to regulate body functions, record biometrics or dispense medicines.

In this paper, we are proposing solution-processed ZnO-based TFTs gated through a phosphate-buffered saline (PBS) solution 10 mM (pH 7.4) put in direct contact with the ZnO surface. The ionic strength of the PBS electrolyte used is 162 mM, while that of human blood serum is 160 mM. As previously outlined, while a few reports are available on water-gated ZnO TFT,³¹ to the best of our knowledge, this is the first time that a liquid electrolyte with an ionic strength comparable to that of a biological fluid is used to gate a ZnO TFT. A full morphological and chemical surface characterization is reported. In addition, a study of the optical and electronic properties of such devices is provided along with the dissolution kinetics, showing how this technology can be useful for “transient” implantable devices.

2. Experimental

2.1 Preparation of the ZnO precursor solution

The ZnO precursor solution (0.1 M) was prepared by dissolving zinc acetate dihydrate, $\text{Zn}(\text{CH}_3\text{COO})_2 \cdot 2\text{H}_2\text{O}$, in ethanol. The solution was stirred for 7 h and at 80 °C, until a transparent, homogenous solution was obtained. The as-prepared precursor solution was deposited *via* spin-coating onto thermally oxidized silicon wafers (Si/SiO₂) for device fabrication.

2.2 Device fabrication

Prior to spin-coating, the Si/SiO₂ substrate was photolithographically patterned with source (S) and drain (D) electrodes (Au/Ti = 50 nm/5 nm). The channel length and width were, unless stated, 10 μm and 10 000 μm respectively. The substrates were cleaned with a piranha solution (3 : 1 mixture of sulfuric acid and hydrogen peroxide) and thoroughly rinsed with solvents of increased polarity (acetone, isopropyl alcohol and deionized water). The precursor solution was deposited on the S–D patterned substrate by spin

coating with a Laurell Technologies WS-650MZ-23NPP/LITE instrument. The thin-film deposition was performed by dispensing a 70 μL drop of precursor solution on the SiO_2 surface and subsequent spinning at 2000 RPM for 50 seconds. The desired film thickness was obtained by repeating the deposition procedure 3 times. Before each further coating, the films were pre-heated at 150 $^\circ\text{C}$ to remove the organic residue. The resulting deposit was calcined at 450 $^\circ\text{C}$ for five hours on a hot plate. All the chemicals and solvents (high quality grade) were purchased by Sigma-Aldrich and used without any further treatment.

2.3 ZnO thin-film characterization

A thermogravimetric analyzer (Perkin Elmer Pyris 6 TGA) was used to study the thermal behavior of $\text{Zn}(\text{CH}_3\text{COO})_2 \cdot 2\text{H}_2\text{O}$ in the temperature range from 30 to 500 $^\circ\text{C}$ with a heating rate of 10 $^\circ\text{C min}^{-1}$ in a 40 mL min^{-1} dinitrogen flow.

The topographical and cross-sectional view micrographs of the films were acquired by a scanning electron microscope (Carl Zeiss SEM system, mod. Sigma). The thickness of the film was evaluated from the cross-sectional SEM image.

The surface chemical composition of the ZnO films, before and after the exposure to water and PBS solutions, was realized with an X-ray photoelectron Thermo VG Theta Probe spectrometer equipped with a micro-spot monochromatized Al $\text{K}\alpha$ source. Both survey scans and high resolution spectra were acquired in the fixed analyzer transmission mode with pass energies of 150 and 100 eV, respectively. The X-ray Photoelectron Spectroscopy (XPS) data were processed with the Avantage software.³⁸ The aliphatic C 1s component fixed at BE values of 284.8 ± 0.1 eV is referenced for calibration of the binding energy (BE) scale. The surface chemical speciation (in at%) of each sample was determined by evaluating the integrated peak areas of the principle photoelectron peaks and the respective sensitivity factor.³⁹

2.4 TFT electrical characterization

The transistor current–voltage (I – V) characteristics were measured, through a pure deionized water or PBS solution gating, with Agilent 4155C and Keithley 4200-SCS Semiconductor Parameter Analyzers. It is worth mentioning that 10 mM PBS solution (pH 7.4) contains a great deal of Na^+ ions. In Fig. 1 a scheme of the device structure is reported.

The output characteristics (I_{DS} vs. V_{DS}) were measured, ranging the source–drain voltage (V_{DS}) between 0 and 0.5 V, while the gate bias (V_{G}) was kept constant for each curve and varied from one curve to the other in 0.1 V steps. The transfer characteristics (I_{DS} vs. V_{G}) were recorded, keeping the drain voltage (V_{D}) constant at 0.5 V. Each current trace was measured in the forward and reverse mode to evidence the occurrence of any hysteresis. The transistor electrical parameters, namely the field-effect mobility (μ), the threshold voltage (V_{T}) and the *on/off* current ratio ($I_{\text{on}}/I_{\text{off}}$), were extracted from the characteristic curves in the saturation regime following an assessed procedure.⁴⁰ All measurements were carried out in ambient air (relative humidity *ca.* 36%, $T = 25$ $^\circ\text{C}$).

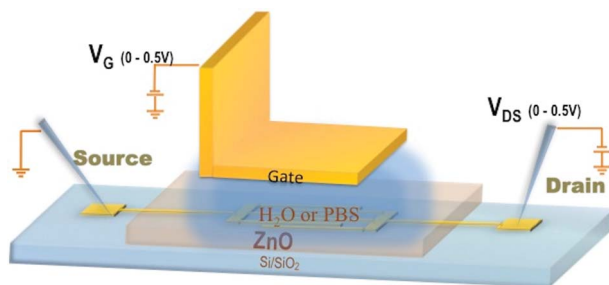


Fig. 1 Electrolyte-gated TFT device structure.

3. Results and discussion

3.1 Thermogravimetric analysis

Thermogravimetric analysis (TGA) was performed in order to study the thermal decomposition of zinc acetate dihydrate ($\text{Zn}(\text{CH}_3\text{COO})_2 \cdot 2\text{H}_2\text{O}$) and the formation of a stable ZnO phase. The thermogram trace and its first derivative at temperatures ranging from 30 to 500 °C are shown in Fig. 2 and in the inset, respectively. The first thermal event is observed at 102.6 °C and is completed at 119 °C with a $\sim 16.7\%$ weight loss. This weight loss can be attributed to the thermal dehydration of zinc acetate dihydrate and more specifically to the loss of the two water molecules. By further increasing the temperature, the decomposition of anhydrous $\text{Zn}(\text{CH}_3\text{COO})_2$ into ZnO occurs at ~ 316.9 °C, and is completed at ~ 353 °C. Beyond this temperature, and up to 500 °C, the formation of a stable ZnO crystal takes place, and no further weight loss is observed. Based on these results, we decided to carry out the calcination at 450 °C, since a stable ZnO phase is obtained. These observations are also in good agreement with previous reports.^{32,41}

3.2 Optical properties

The optical transparency of the ZnO thin film was evaluated on film deposited on a quartz substrate, whose UV-Vis transmittance spectrum is shown in Fig. 3a. The

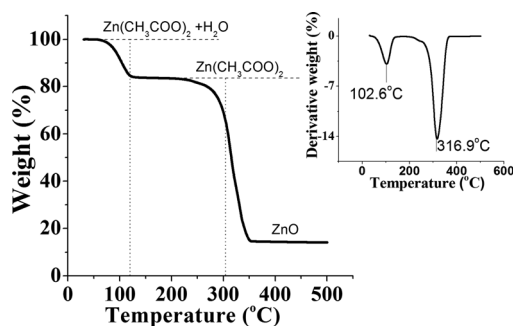


Fig. 2 TG thermogram (30–500 °C) of $\text{Zn}(\text{CH}_3\text{COO})_2 \cdot 2\text{H}_2\text{O}$. Inset: first derivative of the TG thermogram.

optical absorption peak was observed at a wavelength of *ca.* 354 nm which falls in the ultraviolet region of the spectrum, proving the ZnO transparency in the visible region. Considering that ZnO holds a direct band gap transition, the energy gap (E_g) was obtained by using the Bardeen equation:⁴²

$$\alpha h\nu = B(h\nu - E_g)^{1/2} \quad (1)$$

where α is the absorption coefficient and B is a constant.⁴³ The extrapolation from the linear portion to $\alpha h\nu = 0$ (Fig. 3b) results in an $E_g \sim 3.29$ eV.

3.3 X-ray photoelectron spectroscopy surface characterization

X-ray photoelectron spectroscopy (XPS) characterization of the ZnO film was carried out to investigate how the water or PBS solutions influence the surface chemistry. Since the zinc binding energy is not affected by chemical speciation, the O 1s spectral region was studied for the ZnO film, before and after exposure to either water or PBS solution, and the results are shown in Fig. 4. Deconvolution of the O 1s signals showed the presence of four component peaks centered at 530.1 ± 0.2 eV, 531.1 ± 0.2 eV, 532.2 ± 0.2 eV, and 533.3 ± 0.2 eV, labeled as A, B, C and D in Fig. 4. Peak A was assigned to oxygen in the ZnO lattice, peak B was attributed to oxygen in the oxygen-deficient region in the ZnO matrix,^{44,45} peak C was associated to oxygen adsorbed on the surface of the ZnO film, and peak D was assumed to come from the SiO₂ substrate. Interestingly, the four peak components are positioned at the same binding energies in all the samples, and the O 1s XP spectrum before and after water exposure is exactly the same. When the film is exposed to the PBS solution, a different O 1s shape is observed: in particular the intensity ratio B/A is increased, indicating an increase in the number of oxygen vacancies.^{44,45}

3.4 Scanning electron microscopy

The surface morphology and the thickness of the ZnO thin film was evaluated by means of scanning electron microscopy (SEM) analysis. The SEM images, showing the morphological and cross-sectional views of a ZnO thin film deposited on the Si/SiO₂, are shown in Fig. 5a and b, respectively. The film clearly exhibits a granular morphology and has a densely packed structure.⁴⁶ The film thickness

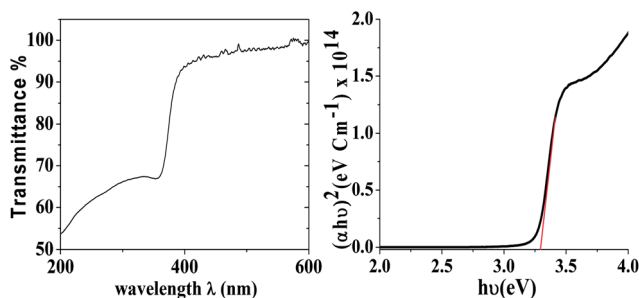


Fig. 3 (a) Optical transmittance spectra of the ZnO thin film deposited on a quartz substrate; (b) optical band gap of the ZnO thin film.

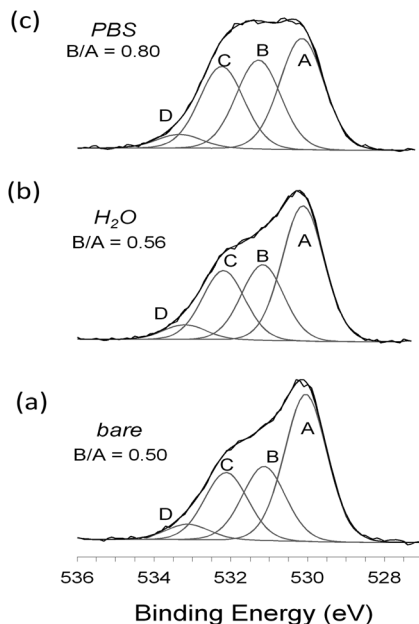


Fig. 4 O 1s XP spectra of the (a) ZnO film and the (b) ZnO sample kept in water, or (c) PBS, for 30 min.

was evaluated from the cross-sectional image as 46 ± 5 nm. In Fig. 5c and d, the SEM images of the ZnO films exposed to water and PBS solutions, respectively, for 14 h under stirring conditions, are reported. ImageJ Software⁴⁷ was used to evaluate the effect of the different electrolytes on the size of the grains. The average grain size, as calculated, was found to be 29 ± 9 nm, 28 ± 6 nm and 26 ± 7 nm for bare ZnO and for the films exposed to water and PBS, respectively. Analysis of the images shows that an overall similar granular morphology is retained after exposure to the two electrolytes, although a slight decrease in the average grain size can be seen for the PBS-exposed film.

3.5 Electrolyte-gated TFT characteristics

Fig. 6 shows the output and transfer characteristics of the pure deionized water and PBS (10 mM, pH = 7.4)-gated ZnO-based thin-film transistors. In Fig. 6a and c the I_{DS} current exhibits well-shaped linear and saturation regions as the V_{DS} bias is swept, and also shows good modulation with the gate bias V_G . The hysteresis shown by the water-gated device is visibly larger. The transfer characteristics in both cases (Fig. 6b and d) were measured at three different integration times, and also in this case the dependence of the integration time is larger for the water-gated device compared to the PBS device. Both these evidences concur to show that more stable electronic behavior is shown by the device operated through the PBS solution. This is an important aspect that will be addressed later on in the text. In the saturation regime the curves follow the well-known analytical expression:

$$I_{DS} = \frac{W}{2L} \mu C_i (V_G - V_T)^2 \quad (2)$$

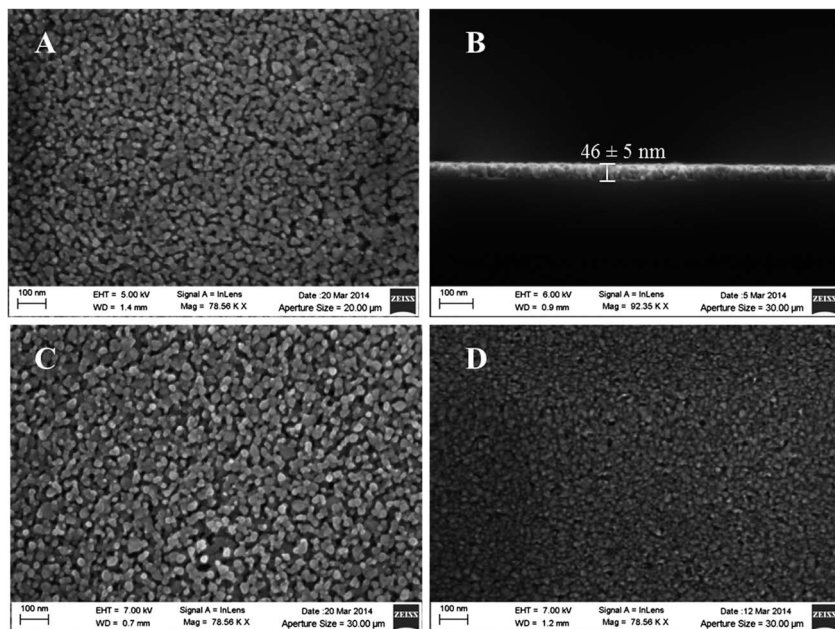


Fig. 5 Topographical scanning electron microscope view of (A) the ZnO thin film, (B) cross-sectional view of the ZnO thin film, (C) ZnO sample kept in water and (D) PBS, for 14 hours under stirring conditions.

The TFT field-effect mobility multiplied by the capacitance per unit area, μC_i , and the threshold voltage (V_T) were derived from the slope (B) and intercept (A) of the linear $\sqrt{I_{DS}}$ vs. V_G plot, according to eqn (3) and eqn (4) reported below.

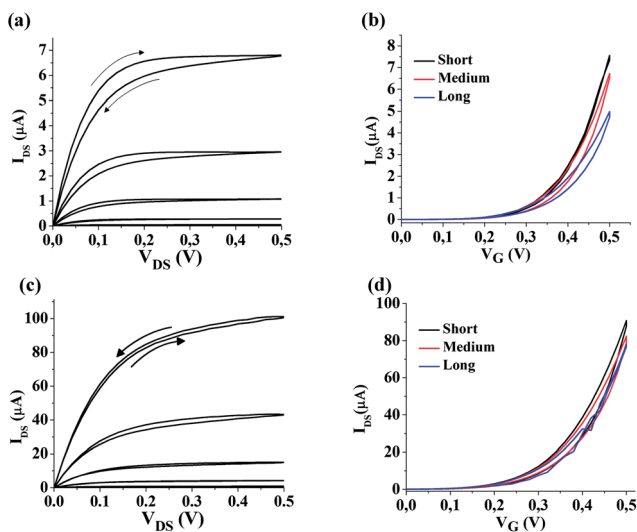


Fig. 6 Current-voltage (I - V) characteristics of the electrolyte-gated ZnO TFT: output (I_{DS} vs. V_{DS}) for (a) water, (c) PBS. Transfer (I_{DS} vs. V_G) for (b) water, (d) PBS at $V_{DS} = -0.5$ V.

$$\mu C_i = \frac{B^2 2L}{W} \quad (3)$$

$$V_T = -\frac{A}{B} \quad (4)$$

The device figures of merit averaged over 3–4 different devices with the relevant uncertainties (one standard deviation) are reported in Table 1. Table 1 also offers a comparison with the literature data concerning ZnO TFTs gated through different solid electrolytes. The comparison is also made with the sole report already published on water-gated ZnO TFTs. To allow for a fair comparison, rather than the mobility data, the μC_i figure of merit is proposed. This is necessary as fully reliable values for the capacitance of liquid or solid electrolytes are not always available.

The measured electrical characteristics obtained from the proposed ZnO devices, summarized in Table 1, present descending field effect behavior. The devices operate at voltages lower than 0.5 V, which is attributed to the electrolyte gating layer. The threshold voltage (V_{th}) is ~ 0.15 V and it is among the lowest reported. The I_{on}/I_{off} ratio is 10^2 for water and 10^3 for PBS. These values are comparable to that of liquid-gated ZnO TFTs.^{31,29} Moreover, the on/off current ratio can be improved by patterning the active channel area. The value of μC_i with PBS as the electrolyte is $1.4 \times 10^{-6} \text{ F V}^{-1} \text{ s}^{-1}$ at the saturation regime, which is similar to that of devices fabricated using a solid electrolyte as the dielectric layer.²⁴

It is worth commenting that the I – V curves of the ZnO thin film exposed to PBS, which is rich in Na^+ ions, exhibit improved electrical characteristics in terms of hysteresis, the I_{on}/I_{off} current ratio and μC_i . More specifically, the hysteresis gap observed in the case of the water-gated ZnO TFT device, reveals the occurrence of charge trapping in the reverse voltage sweep in both the output and transfer characteristics (see Fig. 6a and b). In all cases, the reverse sweep current curve is lower than the forward sweep curve. Furthermore, by reducing the integration time of the gate voltage sweep, an increase in the hysteresis gap is evident, along with a decrease in the maximum on-current (Fig. 6b). It is probable that, for a longer duration of biasing, more charges have time to reach lower energy states and occupy trap sites. On the other hand, when the device is gated with the PBS electrolyte solution, almost hysteresis-free I – V curves are obtained (see Fig. 6c and d). In addition, a higher on current is achieved, meaning that a larger amount of free carriers accumulate in the semiconductor–electrolyte interface. This can be associated to the higher ionic strength of the PBS buffer solution compared to water.

It has been recently demonstrated that Na^+ ions can act as dopants in ZnO, tending to occupy interstitial sites rather than substitutional sites, therefore acting as donors and not as acceptors.⁴⁸ It has also been suggested that the presence of sodium ions can cause a lack of stoichiometry in the ZnO lattice and therefore induce oxygen vacancies.⁴⁵ This is confirmed by the XPS analysis reported in Fig. 4, where an increase in oxygen vacancies is observed in the case of ZnO films exposed to the PBS solution. Indeed, the exposure to Na^+ present in the PBS solution seems to alter the oxide semiconductor lattice on the surface, giving

Table 1 Comparison of the electrical figures of merit of solution-processed electrolyte-gated ZnO TFTs

ZnO	Gate dielectric	μ (cm ² V ⁻¹ s ⁻¹)	V_{DS} (V)	V_G (V)	C_i (μF cm ⁻²)	μC_i (F V ⁻¹ s ⁻¹)	V_T (V)	Slope (A V ⁻² cm ⁻²)	I_{on}/I_{off}	Ref.
Inkjet printing	PS-PMMA-PS and [EMIM] [TFSI]	1.61	0–1.2	0–2	3.8	6.1×10^{-6}	0.97	0.0078	N/A	24
Spray-coated thin film	[HMIM] [FAP]	15.9	0–1.5	–3–1	3.3	5.2×10^{-5}	N/A	0.036	10^3	29
Spin-coated thin film	PS- <i>b</i> -PMMA- <i>b</i> -PS	13	0–0.7	0–1.8	5.08	6.6×10^{-5}	0.62	0.022	10^6	26
Spin-coated thin film	Water	8.8, 1.32	0–0.7	0–0.8	3.20	2.6×10^{-5}	0.36	0.051	10^3	31
Spin-coated thin film	Water	—	0–0.5	0–0.5	—	$(2.3 \pm 0.5) \times 10^{-7}$	0.15 ± 0.04	0.011	3×10^2	This paper
Spin-coated thin film	PBS	—	0–0.5	0–0.5	—	$(1.4 \pm 0.1) \times 10^{-6}$	0.14 ± 0.07	0.028	10^3	This paper

rise to oxygen vacancies. Although oxygen vacancies can produce potential wells that can act as trapping sites,⁴⁴ the excess of free electrons originating from interstitial doping due to Na^+ is such that they can fill the existing trap sites. Moreover, oxygen vacancies can induce more charges in the semiconductor's channel.⁴⁵

3.6 ZnO film dissolution kinetics in water and PBS

The kinetics of ZnO dissolution in aqueous environments were determined by anodic stripping voltammetry (ASV). The Si/SiO₂ substrates, coated by a ZnO film according to the procedure used in the TFT fabrication, were placed in vials containing 3 mL of water or PBS and left under mild stirring on a roller mixer for different time lapses. Reference (blank) slides were left out of the liquids. The amount of residual ZnO at a given time lapse, after the immersion, is defined as the weight percentage of ZnO with respect to the blank. At a given time the slide was removed from the liquid and the coating was dissolved using a wet digestion procedure with nitric–perchloric acids. The solutions obtained after digestion were diluted with deionized water, adjusted to a pH in the 5.0–5.5 range with acetate buffer and dehydrated with a stream of nitrogen for 100 s. The amount of zinc cations dissolved in solution was measured by a differential pulse ASV electrochemical procedure using a three-electrode cell equipped with a hanging mercury drop electrode (HMDE) used as the working electrode, an Ag/AgCl with saturated 3 M KCl reference electrode, and a platinum wire counter electrode. Electrochemical deposition was performed at -0.8 V for 45 s under stirring. After this time the stirrer was switched off, and the oxidation curves were recorded in the potential range from -1.15 to -0.75 V (sweep rate of 0.06 V s⁻¹). Zinc was quantified by the addition of a Zn^{2+} standard solution to the cell.

In Fig. 7 the data are reported for ZnO dissolution in water over a period of 25 h. The zinc actually remaining on the sample after the exposure to water decreases to 46% after 16 h in water, while it decreases down to 25% after exposure to PBS. On the other hand, stable device operation will be shown over a half-hour time lapse later in this manuscript, however the limiting factor is the gating droplet evaporation, not the ZnO film degradation. The actual stable operation time of the device is in fact much longer when comparing the “transient time” of these devices with literature data.³⁷

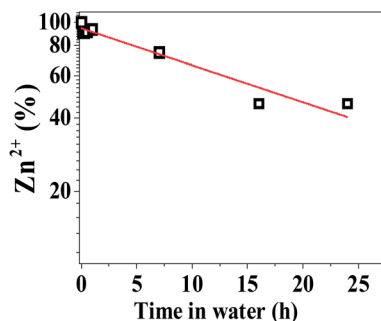


Fig. 7 Dissolution profile of the ZnO film in water.

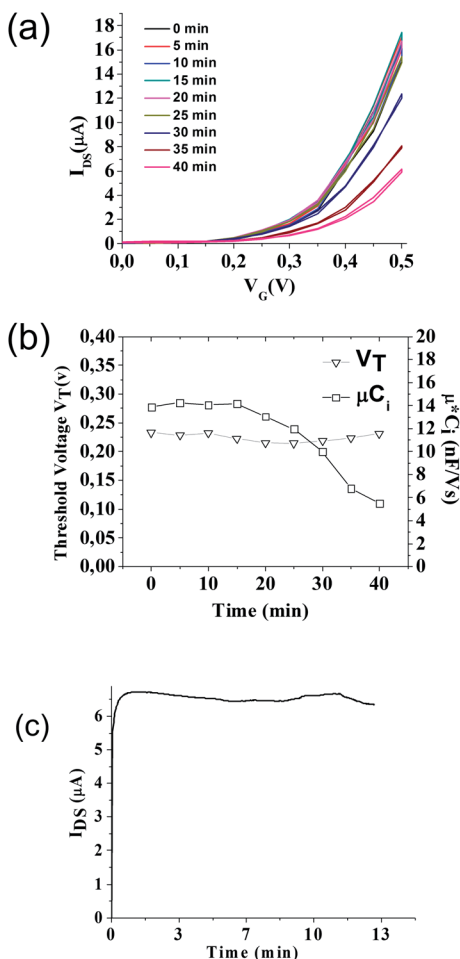


Fig. 8 (a) I – V transfer characteristics of the water-gated ZnO TFT measured repeatedly for 40 min, (b) the relevant V_T , μ^*C_i values, and (c) pulsed transient current measurement of water gated ZnO TFT device.

ZnO appears to react differently under water and PBS solution. The different dissolution processes can be also accounted for by evaluating the degree of hydrophobicity of the ZnO surface after exposure to the two electrolytes. Improved wettability has been ascribed to enhance the dissolution of solid dispersions. Static contact angle evaluation was performed by using a CAM 200 goniometer (KSV Instruments Ltd, Finland) and placing a 2 μL droplet of water or 10 mM PBS on the ZnO film surface at ambient conditions ($T = 25^\circ C$). The measurement was repeated three times by placing the drop on different areas of the same sample, measuring average contact angles of 57 ± 2 for water and 39 ± 6 for PBS, this being more hydrophilic. Interestingly, such a difference cannot be ascribed to differences in the surface tension in the liquid phase because water and PBS have the same value ($71.5 \pm 0.2 \text{ mJ m}^{-2}$) measured using a Du Noüy ring tensiometer (Krüss GmbH, Germany). The difference in the contact angle, therefore, must be ascribed to differences in the solid phase in contact with the liquid droplet, and

this occurrence strongly suggests a doping of the ZnO by ions (presumably Na^+) present in PBS and not in pure water.

3.7 Operational stability of water-gated ZnO TFTs

Another important aspect to be addressed is the operational stability of the proposed ZnO TFT devices. Current instability in thin film transistors under gate voltage biasing is crucial for the practical application of such devices. For this purpose, double transfer characteristic curves were recorded repeatedly, every 5 min, from the moment the device was gated with a water drop until 40 min after. It is important to mention that the channel length and width of the device, used for these measurements, are 2 μm and 60 μm , respectively. As shown in Fig. 8a, the device exhibits stable performance for 25 min. A current decay is observed after half an hour, which can be attributed to possible evaporation of the electrolyte solution. This is further confirmed by the corresponding V_T and μC_i values as a function of time reported in Fig. 8b, where a clear decrease of the μC_i value is in fact observed after 20 min. Pulsed transient measurements⁴⁹ were carried out to examine the dynamic bias stress current instability as well. We used a rectangular wave as a dynamic pulse. The pulse-on time was 10 ms ($V_G = 0.5$ V), while the pulse-off time was 1 s ($V_G = 0$ V) at a constant $V_{DS} = 0.5$ V. As illustrated in Fig. 8c, a stable output current signal in time is observed for approximately more than 10 min. As previously mentioned, the limiting factors to record further the drain current as a function of time are the evaporation of the water droplet and not the degradation of the device.

4. Conclusions

In this study, we have operated an electrolyte-gated ZnO TFT, using a liquid electrolyte with an ionic strength similar to that of physiological fluids. The ZnO precursor solution was prepared by the sol-gel method, while calcination was realized at 450 °C. Low-voltage operation (0.5 V) was achieved, with the electrical figures of merit being in good agreement with those previously reported for electrolyte-gated ZnO TFTs. The carrier density induced in the case of the PBS electrolyte was proven to fill possible trap sites, leading to on-current values higher than the water-gated values. The I - V curves were also hysteresis-free, also exhibiting a slight shift of V_T to a lower voltage value. The enhanced performance of the PBS gating was attributed to interstitial doping of the ZnO matrix by Na^+ ions present in PBS and not in pure water. The proposed mechanism was further confirmed by XPS analysis of the surface chemical composition of ZnO films exposed to water and PBS. Finally, the dissolution profile of ZnO in water and PBS, along with the operational stability of the devices, was studied, showing that this technology can be useful for “transient” implantable devices.

Acknowledgements

Prof. Gaetano Scamarcio is acknowledged for useful discussions. Dr Francesca Intranuovo is acknowledged for the contact angle measurements. The PON project “Laboratorio per lo Sviluppo Integrato delle Scienze e delle Tecnologie dei Materiali Avanzati e per dispositivi innovativi-LABORATORIO SISTEMA” by the

Italian MIUR (Ministry of Education, Universities and Research) is acknowledged for partial support.

References

- 1 R. A. Street, *Adv. Mater.*, 2009, **21**, 2007.
- 2 G. Adamopoulos, S. Thomas, P. H. Wobkenberg, D. D. Bradley, M. A. McLachlan and T. D. Anthopoulos, *Adv. Mater.*, 2011, **23**, 1894.
- 3 E. Fortunato, *Adv. Mater.*, 2012, **24**, 2945.
- 4 D. C. Look, *Mater. Sci. Eng., B*, 2001, **80**, 383.
- 5 D. G. Thomas, *J. Phys. Chem. Solids*, 1960, **15**, 86.
- 6 C. Czekalla, J. Guinard, C. Hanisch, B. Q. Cao, E. M. Kaidashev, N. Boukos, A. Travlos, J. Renard, B. Gayral, D. L. S. Dang, M. Lorenz and M. Grundmann, *Nanotechnology*, 2008, **19**, 115202.
- 7 Z. Li, R. Yang, M. Yu, F. Bai, C. Li and Z. L. Wang, *J. Phys. Chem. C*, 2008, **112**, 20115.
- 8 C. Dagdeviren, S. W. Hwang, Y. Su, S. Kim, H. Cheng, O. Gur, R. Haney, F. G. Omenetto, Y. Huang and J. A. Rogers, *Small*, 2013, **9**, 3398.
- 9 D. H. Kim, Y. S. Kim, J. Amsden, B. Panilaitis, D. L. Kaplan, F. G. Omenetto, M. R. Zakin and J. A. Rogers, *Appl. Phys. Lett.*, 2009, **95**, 133701.
- 10 G. Amin, S. Zaman and A. Zainelabdin, *Phys. Status Solidi Rapid Res. Lett.*, 2011, **5**, 71.
- 11 J. Nishi, F. M. Hossain, A. Takagi, T. Aita, K. Saikusa, Y. Ohmaki, I. Ohkubo, S. Kishimoto, A. Ohtomo, T. Fukumura, F. Matsukura, Y. Ohno, H. Koinuma, H. Ohno and M. Kawasaki, *Jpn. J. Appl. Phys.*, 2003, **42**, L347.
- 12 P. Barquinha, L. Pereira, G. Goncalves, R. Martins and E. Fortunato, *J. Electrochem. Soc.*, 2009, **156**, H161.
- 13 L. Wang, M. H. Yoon, G. Lu, Y. Yang, A. Facchetti and T. J. Marks, *Nat. Mater.*, 2006, **5**, 893.
- 14 P. K. Nayak, J. Jang, C. Lee and Y. Hong, *Appl. Phys. Lett.*, 2009, **95**, 193503.
- 15 Y. H. Hwang, S. J. Seo, J. H. Jeon and B. S. Bae, *Electrochem. Solid-State Lett.*, 2012, **15**, H91.
- 16 Y. H. Kim, J. S. Heo, T. H. Kim, S. Park, M. H. Yoon, J. Kim, M. S. Oh, G. R. Yi, Y. Y. Noh and S. K. Park, *Nature*, 2012, **489**, 128.
- 17 K. K. Banger, Y. Yamashita, K. Mori, R. L. Peterson, T. Leedham, J. Rickard and H. Sirringhaus, *Nat. Mater.*, 2010, **10**, 50.
- 18 B. Sun and H. Sirringhaus, *Nano Lett.*, 2005, **5**, 2413.
- 19 H. Faber, M. Burkhardt, A. Jedaa, D. Kälblein, H. Klauk and M. Halik, *Adv. Mater.*, 2009, **21**, 3099.
- 20 Y. H. Lin, H. Faber, K. Zhao, Q. Wang, A. Amassian, M. McLachlan and T. D. Anthopoulos, *Adv. Mater.*, 2013, **25**, 4346.
- 21 E. Said, X. Crispin, L. Herlogsson, S. Elhag, N. D. Robinson and M. Berggren, *Appl. Phys. Lett.*, 2006, **89**, 143507.
- 22 T. Uemura, M. Yamagishi, S. Ono and J. Takeya, *Appl. Phys. Lett.*, 2009, **95**, 103301.
- 23 M. Magliulo, A. Mallardi, M. Y. Mulla, S. Cotrone, B. R. Pistillo, P. Favia, I. V. Lundin, G. Palazzo and L. Torsi, *Adv. Mater.*, 2013, **25**, 2094.
- 24 K. Hong, S. H. Kim, K. H. Lee and C. D. Frisbie, *Adv. Mater.*, 2013, **25**, 3418.

- 25 Y. Xia, W. Zhang, M. Ha, J. H. Cho, M. J. Renn, C. H. Kim and C. D. Frisbie, *Adv. Funct. Mater.*, 2010, **20**, 587.
- 26 H. Bong, W. H. Lee, D. Y. Lee, B. J. Kim, J. H. Cho and K. Cho, *Appl. Phys. Lett.*, 2010, **96**, 192115.
- 27 S. Bubel, S. Meyer, F. Kunze and M. L. Chabiny, *Appl. Phys. Lett.*, 2013, **103**, 152102.
- 28 H. Yuan, H. Shimotani, A. Tsukazaki, A. Ohtomo, M. Kawasaki and Y. Iwasa, *Adv. Funct. Mater.*, 2009, **19**, 1046.
- 29 S. Thiemann, S. Sachnov, S. Porscha, P. Wasserscheid and J. Zaumseil, *J. Phys. Chem. C*, 2012, **116**, 13536.
- 30 B. Nasr, D. Wang, R. Kruk, H. Rösner, H. Hahn and S. Dasgupta, *Adv. Funct. Mater.*, 2013, **23**, 1758.
- 31 A. A. Naim and M. Grell, *Appl. Phys. Lett.*, 2012, **101**, 141603.
- 32 B. S. Ong, L. Chensha, L. Yuning, Y. Wu and R. Loutfy, *J. Am. Chem. Soc.*, 2007, **129**, 2750.
- 33 O. Yaghmazadeh, F. Cicoira, D. A. Bernards, S. Y. Yang, Y. Bonnassieux and G. G. Malliaras, *J. Polym. Sci., Part B: Polym. Phys.*, 2011, **49**, 34.
- 34 J. Zhou, N. Xu and Z. L. Wang, *Adv. Mater.*, 2006, **18**, 2432.
- 35 M. Irimia Vladu, P. A. Troshi, M. Reisinger, L. Shmygleva, Y. Kanbur, G. Schwabegger, M. Bodea, R. Schwödiauer, A. Mumyatov, J. W. Fergus, V. F. Razumov, H. Sitter, N. S. Sariciftci and S. Bauer, *Adv. Funct. Mater.*, 2010, **20**, 4069.
- 36 C. J. Bettinger and Z. Bao, *Adv. Mater.*, 2010, **22**, 651.
- 37 C. Dagdeviren, S. W. Hwang, Y. Su, S. Kim, H. Cheng, O. Gur, R. Haney, F. G. Omenetto, Y. Huang and J. A. Rogers, *Small*, 2013, **9**, 3398.
- 38 *Thermo Advantage Software v.4.75 copyright*, Thermo Fisher Scientific, 1999–2010.
- 39 R. Pilolli, N. Ditaranto, C. Di Franco, F. Palmisano and N. Cioffi, *Anal. Bioanal. Chem.*, 2012, **404**, 1703.
- 40 L. Torsi, M. Magliulo, K. Manoli and G. Palazzo, *Chem. Soc. Rev.*, 2013, **42**, 8612.
- 41 A. V. Ghule, B. Lo, S. H. Tzing, K. Ghule, H. Chang and Y. C. Ling, *Chem. Phys. Lett.*, 2003, **381**, 270.
- 42 J. Bardeen, F. J. Blatt and L. H. Hall, *Photoconductivity Conf.*, ed. R. Breckenridge, B. Russel and T. Hahn, John-Weiley, New York, 1956.
- 43 S. Ilican, Y. Caglar and M. Caglar, *J. Optoelectron. Adv. Mater.*, 2008, **10**, 2583.
- 44 H. Bong, W. H. Lee, D. Y. Lee, B. J. Kim, J. H. Cho and K. Cho, *Appl. Phys. Lett.*, 2010, **96**, 192115.
- 45 K. Kim, S. Y. Park, K.-H. Lim, C. H. Shin, J.-M. Myoung and Y. S. Kim, *J. Mater. Chem.*, 2012, **22**, 23120.
- 46 S. Singh and P. Chakrabarti, *Superlattices Microstruct.*, 2013, **64**, 283.
- 47 <http://imagej.nih.gov/ij/index.html>.
- 48 C. H. Park, S. B. Zhang and S. H. Wei, *Phys. Rev. B: Condens. Matter Mater. Phys.*, 2002, **66**, 073202.
- 49 K. Manoli, M. M. Patrikoussakis, M. Magliulo, L. M. Dumitru, M. Y. Mulla, L. Sabbatini and L. Torsi, *Org. Electron.*, 2014, **15**, 2372.